Orbital Influence of Asteroid Impact Energies

James Jagielski and Miranda Pietraski

December 2022

1 Introduction

We can predict the age of planetary objects from the amount of craters they have on their surfaces [Stoffler(2006)]. Craters eject material outward, exposing subsurface geology. Mars shows signs of ancient lakes in craters [Hartmann & Neukum(2001)]. Crater features can reveal the energy transferred into the Moon from the impact. The relationship between crater diameter with impact energies and density between the projectile and the target enables crater databases to be converted into impact energies. Thus, we will find distributions of the impact energies of asteroid collisions with the moon [Okeefe & Ahrens(1977)].

Stuart J. Robbins introduced a new database containing a record of and information on over 2 million lunar craters larger than 1-2 kilometers [Robbins(2019)]. The accompanying paper described the methodology used to identify craters and their features using Lunar Reconnaissance Orbiter Cameras such as the Wide Angle Camera and Lunar Orbiter Laser Altimeter. ArcMap software was used to find points along the crater rims. Circle fitting and ellipse fitting is used to approximate the crater, which can also filter out any false craters from human bias. The catalog compared the data to other databases to check its completeness and accuracy [Robbins(2019)].

2 Methods

We compared the distribution of impact energies on the near and far sides of the moon. Further investigation using orbital mechanics allowed us to estimate changes in the Moon's orbit due to asteroid impacts. The calculations made in this study may be a tool in determining the orbital histories of bodies in space.

Our first goal was to examine all craters in the database in terms of their impact energies. The diameter of a crater is related to the kinetic energy of the asteroid and the acceleration due to gravity of the body bring impacted [Okeefe & Ahrens(1977)]. There are several scaling laws that define the relationship between impact energy and crater diameter [Horedt & Neukum(1984)]. We used the modified equation,

$$D = 2.7 \cdot 10^{-2} \rho_p^{1/6} \rho_t^{-1/2} E^{0.28} [1 - 0.095(1 - cos(\theta))] (\frac{g_M}{g})^{\frac{3}{16}}, \quad (1)$$

to derive the amount of energy based on Gault's (1974) crater scaling equation for the moon. The D is the diameter of the asteroid, ρ_p is the density of the asteroid hitting the

moon, ρ_t is the moon's density, E is the energy in the collision, θ is the angle the asteroid is colliding with the moon, and g_M and g are both the gravitational acceleration constant of the moon. We set this ratio equal to 1 because they are gravity scaling parameters that aren't relevant to our investigation. We rearranged the equation to solve for the energy from the impact,

$$E = \left(\frac{D}{2.7 \cdot 10^{-2} \rho_p^{1/6} \rho_t^{-1/2} (1 - 0.095(1 - sin(\theta))(\frac{g_M}{g})^{\frac{3}{16}}}\right)^{\frac{1}{.28}} \tag{2}$$

We are able to determine the diameter of a crater using the Robbins database, but there are other factors in the equation above required to estimate impact energy. One is the angle of collision. Though we do not know this value directly, we can use the ellipticity of the crater to estimate.

With a more elliptical crater, indicative of a non-perpendicular impact angle, the axis ratio of the ellipse is equal to $\frac{1}{sin(\theta)}$ where θ is the angle measured from the horizontal [Bottke(2000)]. This axis ratio is equal to the ellipticity of the crater, which is provided in the Robbins database. To calculate θ, we take the arcsine of the inverse of the ellipticity.

One term in this equation we are not able to determine from crater geometry is the density of the impactor, so we used a constant average density across all craters. Based on the different types of meteorites and their densities and frequencies, the average material density is 3.42 $\frac{g}{cm^3}$. However most asteroids are porous to some degree, so we use a likely average porosity of 34% to determine that the overall average density is 2.26 $\frac{g}{cm^3}$ [Mathias et al.(2017)Mathias, Wheeler, & Dotson]. We also assumed a density of 2.691 $\frac{g}{cm^3}$ constant across the moon's surface [Huang & Wieczorek(2012)].

With these equations, we use a python script to determine the impact energies of all lunar craters of known diameter and ellipticity.

Before we can make full use of the Robbins database, there is some data cleaning we need to do first. Some entries in the database do not contain values for either crater diameter or ellipticity, both of which we need to make calculations. There were relatively few craters with missing data, and we decided to simply exclude any entries where diameter and/or ellipticity are unknown.

With the additional information of latitude and longitude of each crater, we can plot impact energies across the entirety of the moon's surface.

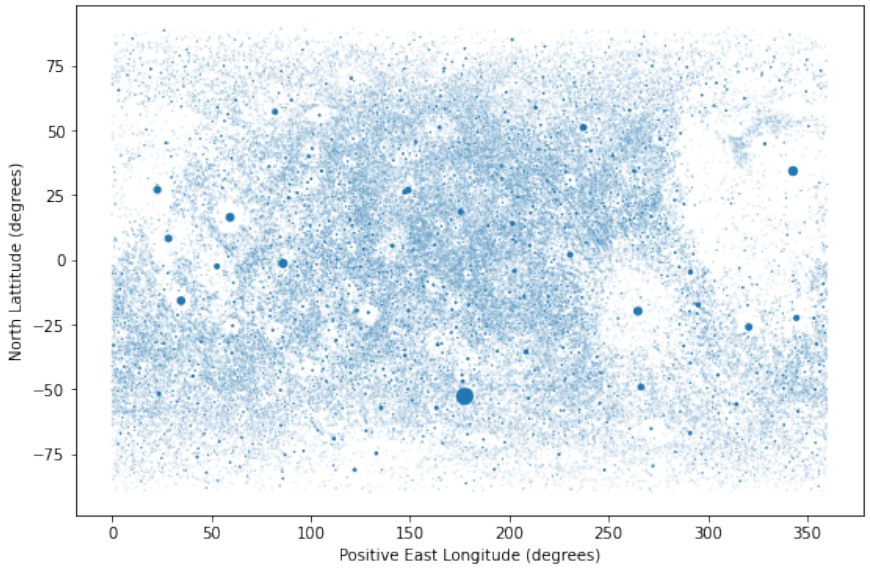

Figure 1: A depiction of crater locations and energies on the surface of the moon. Each point's area is related to the impact energy of that crater. As shown by the many smaller points, the overwhelming majority of craters have small energies compared to the few largest craters. Additionally, it is unexpected that the crater energies taper off to the left, and we are unsure why this is the case.

After plotting what the moon's surface looks like in terms of energy, we can also get a more clear sense of the total distribution of crater energies.

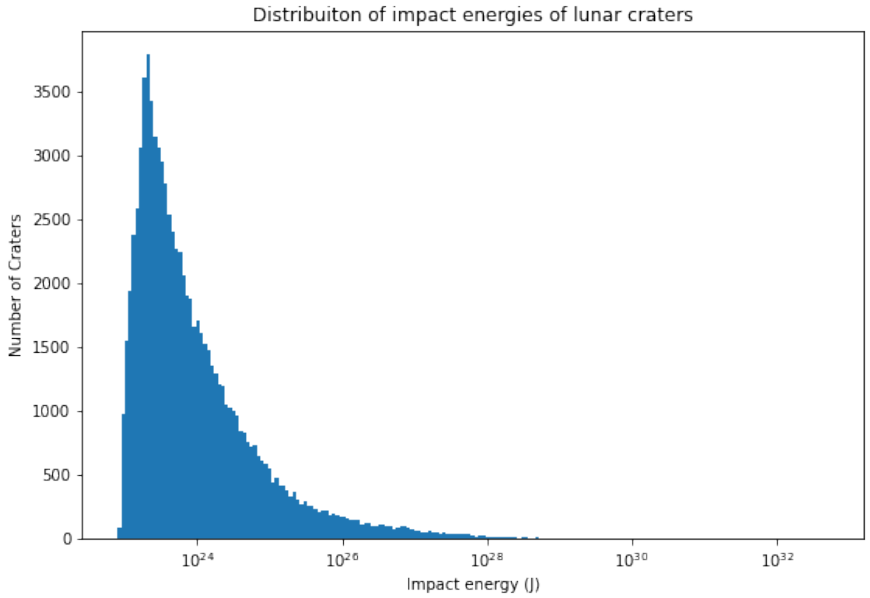

Figure 2: This histogram shows the distribution of crater impact energies. As predicted previously, there are many more craters at the lower end of the total energy range. It is worth noting that the energy axis is on a logarithmic scale due to the large difference between the smallest and largest energies.

These figures are a good representation of impact energies on the moon as a whole, but our goal is to compare the distributions of energy on opposite hemispheres of the moon, specifically the near and far sides.

To separate our data into near and far sides, we need to establish the longitudinal limits of the hemispheres. The prime meridian of the moon is conventionally set to the meridian most facing the earth, or the exact center of the light side [Walden et al.(2002)Walden, McGown, York, & Billings]. Based on this information, we can say that all points between 90° and 270° positive east longitude are on the far side, the rest being on the near side. Therefore, we can sort our data into two categories based on longitude range and examine the statistics of each separately.

2.1 Orbit Determination

With the energy and angle of impact from the asteroids we were interested in how these collisions would affect the orbit of the moon. Orbit determination is a well studied area and there are many methods to determining the path. We are using the Kepler orbit without the influence of time. We are simply manually assigning angles as our independent variable.

2.1.1 2D orbital modeling

We started with the two body problem in the 2-D domain to simplify our model. The equation we used was,

$$r(t) = \frac{a \cdot (1 - e^2)}{(1 + e \cdot cos(f(t))}, \tag{3}$$

where a is length of the semi-major axis (the long axis in an ellipse), e is eccentricity (how elliptic the orbit is) represented by a number $0 \leq e \leq 1$, and f is the true anomaly (θ between periapsis and the current position) [Curtis(2008)]. We did not include the time domain in our project, so we swept f for $0° \leq \theta \leq 360°$. This problem has a few assumptions: the mass of the body is concentrated at a point and the second assumption is earth is a spherical planet. Equation 3 is derived by the equations below. In this problem, we are able to have the center of mass of the entire system serve as the origin of our reference frame. This will allow us to get the position of the moon without worrying about the position of the earth. Thus, the barycenter becomes,

$$\vec{R}_{CM} = \frac{\vec{R}_1 m_1 + \vec{R}_2 m_2}{m_1 + m_2} = 0, \tag{4}$$

where $\vec{R}_1$ and m_1 are the position and mass of object 1 and $\vec{R}_2$ and m_2 are the position and mass of object 2. We assign $\vec{r}_{12}$ as the position of $\vec{R}_2$ relative to the position of $\vec{R}_1$, so we get the result,

$$\vec{r}_{12} = \vec{R}_2 - \vec{R}_1, \tag{5}$$

which we can use to solve for the absolute value of $\vec{R}_1$ and $\vec{R}_2$. Thus, we get the equations,

$$\vec{R}_1 = -\frac{m_2}{m_1 + m_2}\vec{r}_{12}, \tag{6}$$

$$\vec{R}_2 = \frac{m_1}{m_1 + m_2}\vec{r}_{12}, \tag{7}$$

which gives the absolute position of $\vec{R}_1$ and $\vec{R}_2$ in reference to the barycenter. Using the forces caused by both masses on each other we can solve for the two body motion,

$$\ddot{\vec{r}}_{12} = -\frac{G(m_1 + m_2)}{||\vec{r}_{12}||^3}\vec{r}_{12}, \tag{8}$$

where $\ddot{\vec{r}}_{12}$ is the acceleration $\vec{r}_{12}$ position and G is the gravitational constant. This equation of motion gives us six differential equations, three for position and three for velocity. This set up of the two body problem allows us to solve for the standard gravitational parameter of the moon (μ), which is a constant. The equation of (μ) can simplify down to,

$$\mu = Gm_{moon}, \tag{9}$$

where m_{moon} is the mass of the moon. This equation is derived from the equations above. Now we can start to define the components and variables that describe the position of the orbit in respect to the true anomaly. Angular momentum is normal to the orbit created by,

$$\vec{h} = \vec{r} \times \dot{\vec{r}}, \tag{10}$$

where $\dot{\vec{r}}$ can be replaced with the velocity vector ($\vec{v}$). We then define the eccentricity vector as,

$$\vec{e} = \frac{1}{\mu}(\dot{\vec{r}} \times \vec{h} - \mu\frac{\vec{r}}{||\vec{r}||}), \tag{11}$$

which needs to be proven to be constant. This proof has already been proven, thus,

$$e = ||\vec{e}||. \tag{12}$$

The eccentricity (e) of the moon is 0.0554, which means the moon is close to a circular orbit because 0 is a perfect circular orbit. With these values we can measure the position with respect to the eccentricity vector because it points towards the periapsis of the orbit. We get the angle of f with the equation,

$$cos(f(t)) = \frac{\vec{r}(f(t)) \cdot \vec{e}}{r(f(t))e}, \tag{13}$$

and we can derive the position as a function of f from this equation. We then get the polar equation,

$$r(f(t)) = \frac{h^2}{\mu(1 + ecos(f(t)))}. \tag{14}$$

We then need to get the semi-latus rectum,

$$p = \frac{h^2}{\mu} \tag{15}$$

which is when f is at 90° and p represents the semi-latus rectum. We can use p to solve for the apogee of the orbit by substituting f with π into equation 14, which yields,

$$a = \frac{p}{1-e}, \tag{16}$$

which a is the semi-major axis of the orbit. We can rearrange the equation to get p, isolated,

$$p = a(1-e^2), \tag{17}$$

so we can substitute this equation back into the polar equation 14. Thus, we then produce the equation 3, which we used for the 2-D polar plot of the moon's orbit [Taylor(2005)].

variable	value	unit
e	0.0554	unit less
μ	$4.903 \cdot 10^3$	$\frac{km^3}{s^2}$
a	384400	km

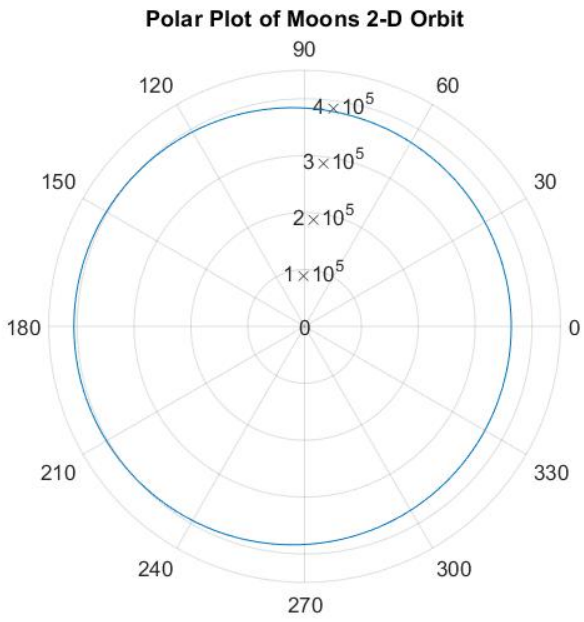

Figure 3: The figure of the orbit is positioned at each degree which is denoted by the numbers wrapping around the plot. The distance from the center is denoted by the values from 60° and 90° measured in kilometers. The plot places the perigee at 363,295 km and apogee at 405,502 km. The overall orbit appears to be what is expected in the result because the eccentricity is low.

We measured the accuracy of the plot by comparing the real values: 363,396 km at perigee and 405,504 km at apogee to the plot values. There is .03% error for the perigee and 0% error for the apogee.

2.1.2 3D orbital modeling

The modeling of 3D orbits relies heavily on coordinate systems. In order to convert between coordinate systems we will utilize the 3D rotational matrices,

$$R_1(\phi) = \begin{bmatrix} 1 & 0 & 0 \\ 0 & cos\phi & -sin\phi \\ 0 & sin\phi & cos\phi \end{bmatrix} R_2(\theta) = \begin{bmatrix} cos\theta & 0 & sin\theta \\ 0 & 1 & 0 \\ -sin\theta & 0 & cos\theta \end{bmatrix} \quad R_3(\varphi) = \begin{bmatrix} cos\varphi & -sin\varphi & 0 \\ sin\varphi & cos\varphi & 0 \\ 0 & 0 & 1 \end{bmatrix}, \tag{18}$$

where $R_1(\phi)$ is the roll (X-axis), $R_2(\theta)$ is the pitch (Y-axis), and $R_3(\varphi)$ is the yaw (Z-axis). We have our position (r) in the satellite normal frame, so we need to convert it to perifocal coordinates through the rotational matrices. The conversion is then set up as,

$$\vec{r}_{PQW} = R_3(f) \begin{bmatrix} r \\ 0 \\ 0 \end{bmatrix}_{SN}, \tag{19}$$

and we rotated around the z-axis, so we can input f as the angle. This results in,

$$\vec{r}_{PQW} = \begin{bmatrix} rcosf \\ rsinf \\ 0 \end{bmatrix}, \tag{20}$$

which can take every r from our 2D orbit and convert it into the PQW coordinate frame. We can then rotate the perifocal coordinates of the position through three rotations. In order to do this we will define the three orbital elements: right ascension of the ascending node (Ω), argument of periapsis (ω), and inclination (i). The right ascension is the angle between the vernal equinox (x-axis of the ECI frame) and the ascending node. The argument of periapsis is the angle between the ascending node and the perigee. The ascending node refers to the point in an orbit where the object crosses the equatorial plane going from south to north. The inclination is the angle between the orbital plane and the equatorial plane. These elements all influence the 3D model of the orbit. We can rotate the $\vec{r}_{PQW}$ coordinates with our 3D rotational matrices. We will rotate ω about the z-axis, rotate i about the x-axis, and then rotate Ω around the z-axis [Prussing & Conway(1993)]. The rotation equations become,

$$R_{PQW\rightarrow ECI} = \begin{bmatrix} cos\Omega & -sin\Omega & 0 \\ sin\Omega & cos\Omega & 0 \\ 0 & 0 & 1 \end{bmatrix} \begin{bmatrix} 1 & 0 & 0 \\ 0 & cos(i) & -sin(i) \\ 0 & sin(i) & cos(i) \end{bmatrix} \begin{bmatrix} cos\omega & -sin\omega & 0 \\ sin\omega & cos\omega & 0 \\ 0 & 0 & 1 \end{bmatrix} \tag{21}$$

$$= \begin{bmatrix} cos\Omega cos\omega - sin\Omega sin\omega cos(i) & -cos\Omega sin\omega - sin\Omega cos\omega cos(i) & sin\Omega sin(i) \\ sin\Omega cos\omega + cos\Omega sin\omega cos(i) & -sin\Omega sin\omega + cos\Omega cos\omega cos(i) & -cos\Omega sin(i) \\ sin\omega sin(i) & cos\omega sin(i) & cos(i) \end{bmatrix}. \tag{22}$$

The rotational matrices we are converting R_{PQW} with, look different than the 3D rotational matrices because we needed to take their inverses,

$$\vec{r}_{PQW} = R_3(-\omega)R_1(-i)R_3(-\Omega)\vec{r}_{ECI}, \tag{23}$$

but this equation is the rotations for converting the ECI coordinates to PQW, so we take the inverses and the equation becomes,

$$\vec{r}_{ECI} = R_3(\Omega)R_1(i)R_3(\omega)\begin{bmatrix} rcosf \\ rsinf \\ 0 \end{bmatrix}_{PQW}. \tag{24}$$

The final rotation can simplify further to the equation,

$$\vec{r} = \begin{bmatrix} r(cos\Omega cos(\omega+f)) - sin\Omega sin(\omega+f)cos(i)) \\ r(sin\Omega cos(\omega+f)) + cos\Omega sin(\omega+f)cos(i)) \\ rsin(\omega+f)sin(i) \end{bmatrix} \tag{25}$$

2.1.3 3D plots

variable	value	unit
i	5.16	$\theta°$
Ω	317.7	$\theta°$
ω	318.15	$\theta°$

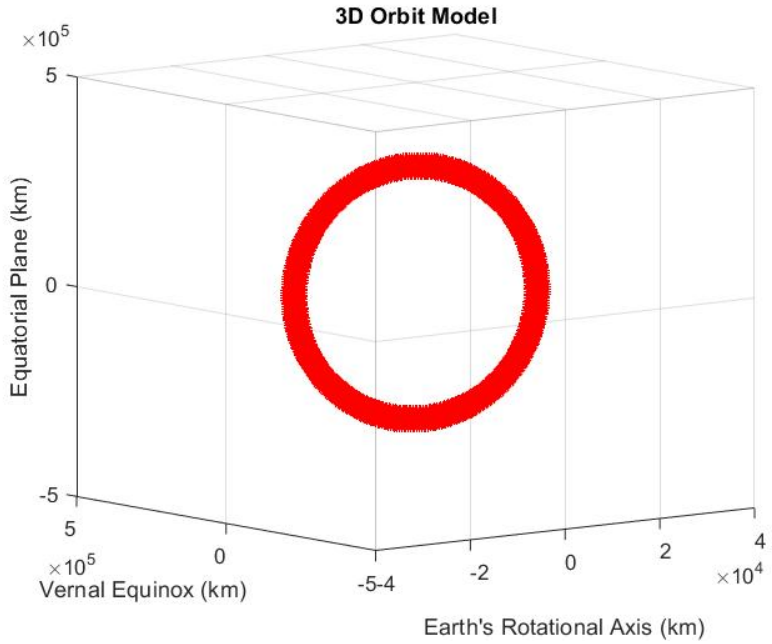

Figure 4: This figure gives a top down view of the 3D orbit. We checked the dimensions of the orbit with the moons actual orbit and they aligned closely.

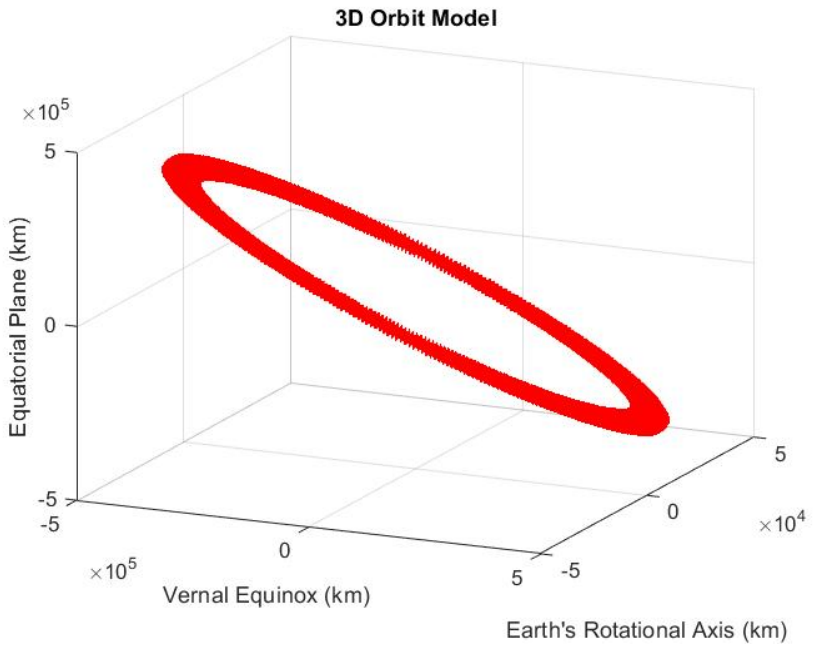

Figure 5: We included this figure to give a sense of what the orbit appears to be to give a better perspective. The higher edge of the orbit is further away. The angle of the orbit seems to be higher than expected, but the values are validated.

2.1.4 Changes in Orbital elements

Changes in orbit are extremely commonly caused by reasons like drag and non-spherical planetary objects. In our instance, we modeled constant forces from asteroids colliding with the moon. We got all the data from the Robbins database, previous work done thus far, or they are assumptions we have created. We are maintaining the assumption of constant density for the asteroids at $2260\frac{g}{cm^3}$, assuming the asteroids are perfectly spherical, and the length of the impact is 2 seconds. We needed to convert our impact energies to force vectors. We started by calculating the volume of each asteroid based on the diameters,

$$V = \frac{4}{3}\pi(\frac{D}{2})^3, \tag{26}$$

where V is the volume of the asteroid and D is the diameter of the asteroid. We then got the mass of the asteroids by the density equation $m = \rho \cdot V$. This gives us all the variables to isolate velocity from the kinetic energy equation,

$$v = \sqrt{\frac{2K}{m}}, \tag{27}$$

with v as velocity and K as kinetic energy. We can now get our force by the impulse of the collision,

$$\vec{F} = \frac{m\Delta v}{\Delta t}, \tag{28}$$

where the Δv is just $-v$ and Δt is 2 seconds, which we assumed for every impact. The next step is breaking down the force into the RTN coordinate system. Since the moon is tidally locked in it's orbit we don't need to worry about the rotation of the coordinate system as the RTN frame will always remain constant. Thus, we can apply the conversion equations,

$$R = F\cos\theta\sin\phi \tag{29}$$
$$T = -F\cos\theta\cos\phi \tag{30}$$
$$N = F\sin\theta, \tag{31}$$

with θ as the angle from $\vec{F}$ to the RT plane and ϕ as the angle between $\vec{F}$ and the NT plane. With our force broken down into the RTN components, we can calculate the change in each orbital element with the following equations,

$$\dot{a} = 2\sqrt{\frac{a^3}{\mu(1-e^2)}}[eRsinf + T(1+ecosf)], \tag{32}$$

which calculates the change in length of the semi-major axis of the ellipse. The next equation is,

$$\dot{e} = \sqrt{\frac{a(1-e^2)}{\mu}}[Rsinf + T(cosf + cosE_{ecc})], \tag{33}$$

to calculate the change in the eccentricity of the orbit. This equation involves the new variable eccentric anomaly E_{ecc}, which can be derived from f. The equation is,

$$E_{ecc} = 2\,tan^{-1}\sqrt{\frac{1-e}{1+e}}\tan\frac{f}{2}, \tag{34}$$

which we can plug in directly into $\dot{e}$. Next we can also solve for the 3D elements,

$$\frac{d}{dt}i = \sqrt{\frac{a(1-e^2)}{\mu}}\frac{N\cos(w+f)}{1+ecosf}, \tag{35}$$

$$\dot{\Omega} = \sqrt{\frac{a(1-e^2)}{\mu}}\frac{Nsin(w+f)}{sin\,i(1+e\,cosf)}, \tag{36}$$

$$\dot{\omega} = -\dot{\Omega}\,cos\,i\sqrt{\frac{a(1-e^2)}{e^2\mu}}(-Rcosf + T\frac{(2+ecosf)sinf}{1+e\,cosf}), \tag{37}$$

which you might notice are all the derivative with respect to time [Danby(1992)]. These equations are meant to be the rate of change over time and for secular perturbations like the ones we are measuring. You would integrate in respect to time, but we used the equations as the rate of change with respect to f. All of these equations are derived using many of the components in this paper.

3 Results

We used the Robbins database for the location of the craters to compare the impact energies on the near and far sides of the moon. For each side of the moon, we calculated the individual energies of the craters. Based on the individual energies, we calculated the total energy and the average energy on the near and far sides of the moon. The far side of the moon has a total impact energy of $4.90 \cdot 10^{32}$ J while the near side has a total impact energy $1.54 \cdot 10^{32}$ J. As we can see, all the craters on the far side of the moon show over 3 times the impact energy of all the craters on the near side. To understand these numbers a little more clearly, we can look at the distribution on each side in more detail.

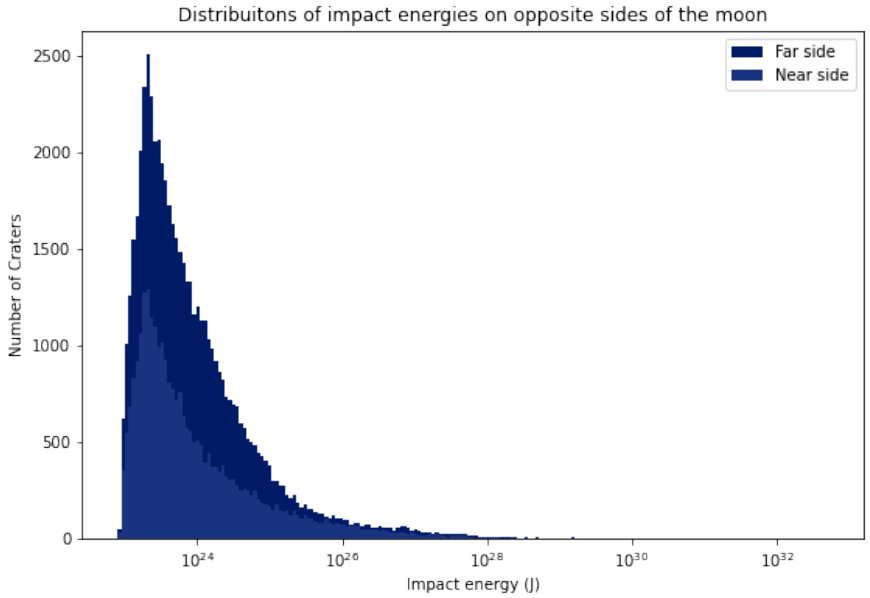

Figure 6: Based on the data separated by hemisphere, we can see that the distributions of craters on opposite sides of the moon are similar. There are 55579 craters on the far side and 27474 on the near side. The mean impact energies are also similar ($8.82 \cdot 10^{27}$ J on the far side and $5.59 \cdot 10^{27}$ J on the near side.) There is more difference between standard deviations ($1.81 \cdot 10^{30}$ J on the far side and $3.39 \cdot 10^{29}$ J on the near side.)

The general distributions of craters on both sides of the moon are not too dissimilar. The main contributing factor to the greater impact energy on the far side of the moon is the greater frequency with which the far side is impacted. The far side of the moon has a greater number of craters, but the amount of energy from craters individually is not significantly different.

4 Conclusion

Based on our results, the far side of the moon is impacted much more frequently and with slightly more energy than the near side. The difference in number of craters is substantial and points to there being some feature of the moon and/or its position relative to the earth

that makes impacts more likely on the far side, or diminishes evidence of impacts on the near side. A possible reason for this is the difference in maria on the near and far sides. The near side's surface has significantly more maria as a result of volcanic activity where the crust is thinner. It may be that lava flow as a result of the maria's formation also obscured many craters on the near side [Jones et al.(2022)Jones, Evans, Johnson, Weller, Andrews-Hanna, Tikoo, & Keane].

The assumptions of uniform density on the surface of the moon and the average density for every asteroid will inhibit the accuracy of our results, but they yield results that are sufficient for modeling purposes.

We can continue this process to compare more planetary objects to see how impact energies have influenced their orbital elements. Unfortunately, we were not able to get accurate results depicting orbital changes due to asteroid impacts. We believe the calculations for the changes were off by such a large magnitude because we didn't make the calculations in respect to time due to not having the time for the creation of the craters. However, if we were to build an accurate method upon these foundations, it may be possible to abstract this further and track the history of orbits from these planetary objects. With the ability to track the path of planetary objects in orbits we can both look back at the position of planetary objects in the universe and make predictions for what the universe will look like in the future.

References

[Bottke(2000)] Bottke, W. 2000, Icarus, 145, 108, doi: 10.1006/icar.1999.6323

[Curtis(2008)] Curtis, H. D. 2008, Orbital mechanics for engineering students, 1st edn., Elsevier Aerospace engineering series (Amsterdam Heidelberg: Elsevier Butterworth Heinemann)

[Danby(1992)] Danby, J. M. A. 1992, Fundamentals of celestial mechanics. https://ui.adsabs.harvard.edu/abs/1992fcm..book.....D

[Hartmann & Neukum(2001)] Hartmann, W. K., & Neukum, G. 2001, Space Science Reviews, 96, 165, doi: 10.1023/A:1011945222010

[Horedt & Neukum(1984)] Horedt, G. P., & Neukum, G. 1984, Earth, Moon and Planets, 31, 265, doi: 10.1007/BF00058905

[Huang & Wieczorek(2012)] Huang, Q., & Wieczorek, M. A. 2012, Journal of Geophysical Research: Planets, 117, doi: 10.1029/2012JE004062

[Jones et al.(2022)Jones, Evans, Johnson, Weller, Andrews-Hanna, Tikoo, & Keane] Jones, M. J., Evans, A. J., Johnson, B. C., et al. 2022, Science Advances, 8, eabm8475, doi: 10.1126/sciadv.abm8475

[Mathias et al.(2017)Mathias, Wheeler, & Dotson] Mathias, D. L., Wheeler, L. F., & Dotson, J. L. 2017, Icarus, 289, 106, doi: 10.1016/j.icarus.2017.02.009

[Okeefe & Ahrens(1977)] Okeefe, J. D., & Ahrens, T. J. 1977, Lunar and Planetary Science Conference Proceedings, 3, 3357. https://ui.adsabs.harvard.edu/abs/1977LPSC....8.3357O

[Prussing & Conway(1993)] Prussing, J. E., & Conway, B. A. 1993, Orbital Mechanics (Oxford University Press)

[Robbins(2019)] Robbins, S. J. 2019, Journal of Geophysical Research (Planets), 124, 871, doi: 10.1029/2018JE005592

[Stoffler(2006)] Stoffler, D. 2006, Reviews in Mineralogy and Geochemistry, 60, 519, doi: 10.2138/rmg.2006.60.05

[Taylor(2005)] Taylor, J. R. 2005, Classical Mechanics (University Science Books)

[Walden et al.(2002)Walden, McGown, York, & Billings] Walden, B., McGown, R. D., York, C. L., & Billings, T. L. 2002, Lunar "West Pole" Prime Meridian. https://ui.adsabs.harvard.edu/abs/2002spro.conf..115W